Etch Rate Dependence on Crystal Orientation for Lithium Niobate

Andrew B. Randles, Shuji Tanaka and Masayoshi Esashi
Department of Nanomechanics, Graduate School of Engineering, Tohoku University
Sendai, Japan 980–8579
Email: arandles@mems.mech.tohoku.ac.jp

***Abstract*—This paper presents experimental data for the etch rate of lithium niobate ($LiNbO_3$) as a function of crystal orientation. The etching characterization is a fundamental technology needed for the fabrication of new sensors, actuators or other new devices. In this study, 30 mm spheres of $LiNbO_3$ were etched in hydrofluoric acid and in a solution of hydrofluoric and nitric acids, to determine the etch rate dependence on crystal orientation. It was found that the maximum etch rate was on the –Z face and the etching showed a three-fold symmetry about the Z axis. The Wulff-Jaccodine method as well as the data collected from the etched spheres were used to predict the etched shape of a wafer. The predicted shape agreed with that found during etching.**

I. Introduction

Lithium niobate ($LiNbO_3$) is a ferroelectric material used extensively in optics and surface acoustic wave (SAW) devices. $LiNbO_3$ is not typically used for microelectromechanical systems (MEMS) applications, partly because the bulk micromachining of $LiNbO_3$ is not as well understood as it is with other materials. Data for the full etch rated dependence on crystal orientation for both silicon (Si) and quartz have been published, which has allowed for the simulation of the etching of these crystals [1], [2], [3]. Similar data has also been published for germanium [4], [5], [6]. With etch simulators, the design of devices with complex structures is possible.

A few devices have been fabricated, which use surface micromachined MEMS technology combined with SAW technology [7], [8], [9]; however, very few devices have been fabricated by combining SAW technology with bulk micromachining of $LiNbO_3$. This is partly due to the unknown etching characteristics of $LiNbO_3$ on different crystal planes. This could be addressed with the development of a full etching map for $LiNbO_3$.

An easy way to examine the etch rate dependence on crystal orientation is a wagon wheel method [10]. When the wagon wheel mask was used in our experiments, the undercut of Cr in Cr/Au masks made the results unclear. In addition, it is only performed on a single crystal cut, and many characterizations would need to be done for each crystal cut. The limitations of the wagon wheel method can be addressed by etching a sphere and determining the etch rate on all crystal faces at once.

In this study, the etch rate dependence of $LiNbO_3$ on crystal orientation was investigated using $LiNbO_3$ spheres. We obtained the data from the etched spheres, and used the Wulff-Jaccodine method to predicted the exposed crystal planes and profiles of etched wafers.

II. Process

The process used for etching and measuring $LiNbO_3$ spheres is similar to the process developed by Sato *et al.* [2], [3]. The differences between their process and the process used for $LiNbO_3$ are that a mask was not sputtered on the orientation flats, and a more complete sphere was used. For the experiments performed with Si, Sato *et al.* only used a hemisphere of Si because of the etch symmetry. $LiNbO_3$ does not share a similar etch symmetry to Si, so a sphere with a measurable region from 0° to 150° was used to gain a more complete etch profile for the crystal (Fig. 1(a, b)). In addition, a sputtered mask was not used, in order to minimize temperature gradients in the spheres resulting from sputtering. Temperature gradients in the sphere could have caused the sphere to break, because of internal stresses.

A $LiNbO_3$ ingot, which was 76.4 mm in diameter and 35 mm in thickness, was polished into three spheres. The spheres were 30 mm in diameter with an orientation flat polished on the +X face, where two holes drilled in the orientation flat. The diameter of the sphere was chosen to be 30 mm, because it allowed for etches of 50 to 60 μm while still maintaining good differentiation of adjacent crystal planes [2]. For the experiments, a large sphere is best because it allows for deep etches and more resolution in determing individual crystal cuts. However, large single crystal spheres are expensive, so this limited the size of the spheres that were used.

The orientation flat on the +X face was chosen because it is known that $LiNbO_3$ has similar etching characteristics on the ±X faces, while there is differential etching on both the ±Y and ±Z faces. Placing the orientation flat on the +X face does not result in a significant loss of data. The holes drilled into the orientation flat determined the orientation of the Y axis. One hole was drilled in the center of the orientation flat and the second was offset from the central hole, indicating the +Y direction. When measuring a sphere, it was placed on a custom built stand with pegs which went into these holes. There was an orientation flat machined perpendicular to the –Y face on the stand. That orientation flat was probed by a Mitsutoyo Legex 707, a computer numerically controlled (CNC) cordinate measuring machine (CMM), to determine the

1051-0117/07/$25.00 ©2007 IEEE

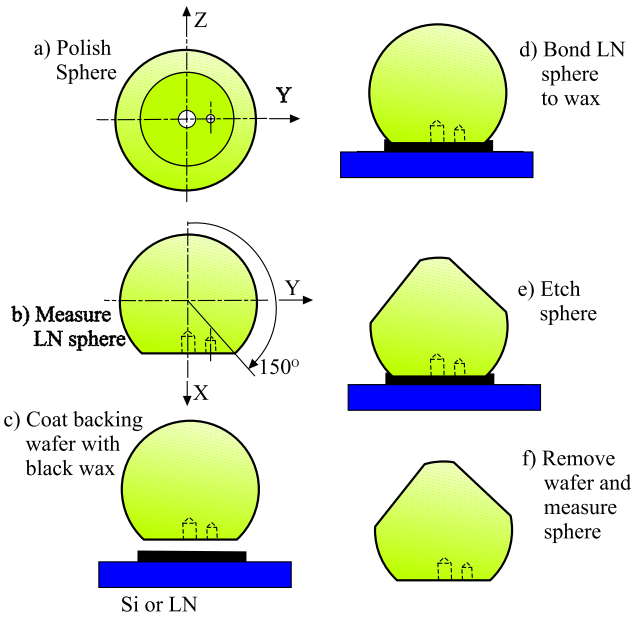

Fig. 1. Process for the orientation etch rate dependence experiments.

TABLE I
ETCH CONDITIONS USED FOR DIFFERENT SPHERES. THE SOLUTION CONCENTRATIONS WERE 49 WT% HF AND 70 WT% HNO_3. THE MIXING RATIOS WERE BY VOLUME.

Condition #	*Etch Solution*	*Etch Temperature*	*Etch Time*
1	HF	80 °C	2 h
2	HF	80 °C	3 h
3	1:2 HF:HNO_3	80 °C	1 h
4	1:2 HF:HNO_3	80 °C	2 h
5	1:2 HF:HNO_3	90 °C	1 h

orientation of the sphere with respect to the coordinate system used by the CNC CMM.

The experimental procedure is shown in Fig. 1. To protect the orientation flat during etching, black wax and a support wafer were used. When the etch solution was hydrofluoric and nitric acids (HF:HNO_3), the Si backing wafer was replaced with a $LiNbO_3$ backing wafer (Fig. 1(c)). Otherwise, a self catalatic etching of the Si happens. The wafer supported the sphere in the etchant, and helped to maintain the integrity of the black wax. The etching setup used a hot water bath to heat the etchant and the sphere in a dry beaker. When the sphere and the etchant had reached the experiment's prescribed temperature, the sphere was placed in the etchant. This was done to minimize temperature gradients in the sphere and to minimize temperature variations in the etchant when the sphere was placed in the etchant. The etchant was not stirred. After removing the backing wafer, the samples were measured in the CNC CMM. The sphere was measured every 2°, which resulted in over 9,000 data points for each etch condition.

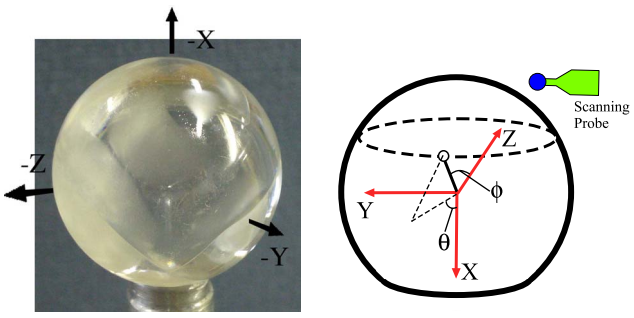

(a) Etched sphere (b) Angle definition for the sphere

Fig. 2. Photograph of an etched sphere and angle definition .

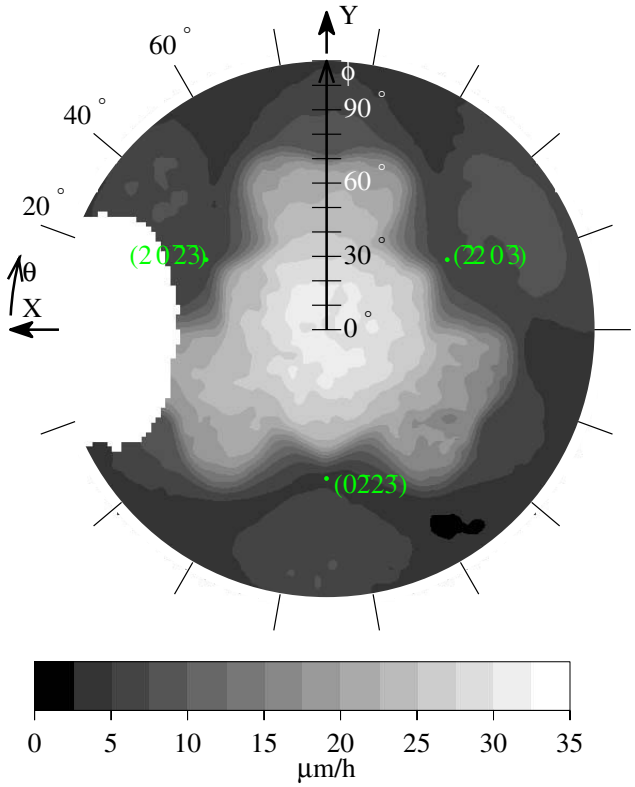

Fig. 3. –Z hemisphere etch rate of $LiNbO_3$ in HF at 80 °C, etched for two hours.

Several different etching conditions were tested; as listed in Table I. The same sphere was used for contions 1 and 2, and a another sphere was used for conditions 3 and 4. After etching and measuring the first condition, the process was repeated again.

III. RESULTS

Fig. 2(a) shows an example of an etched sphere. The etch rate distributions are shown in Figs. 3 and 4 for conditions 1 and 4, respectively. The angles θ and ϕ are defined as shown in Fig. 2(b). In Figs. 3 and 4, the radius of the circle corresponds to ϕ in Fig. 2(b), and the in-plane angle of the

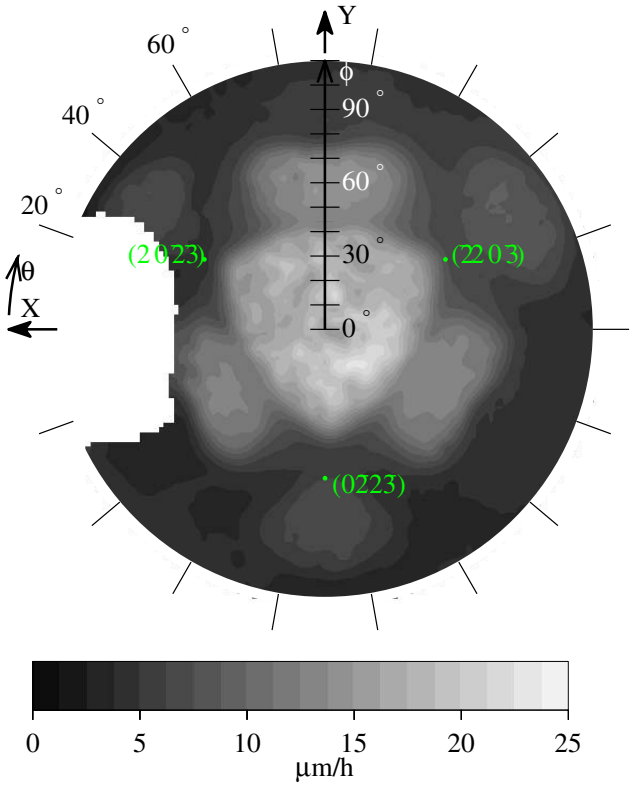

Fig. 4. –Z hemisphere etch rate of $LiNbO_3$ in HF:HNO_3 at 80 °C, etched for two hours

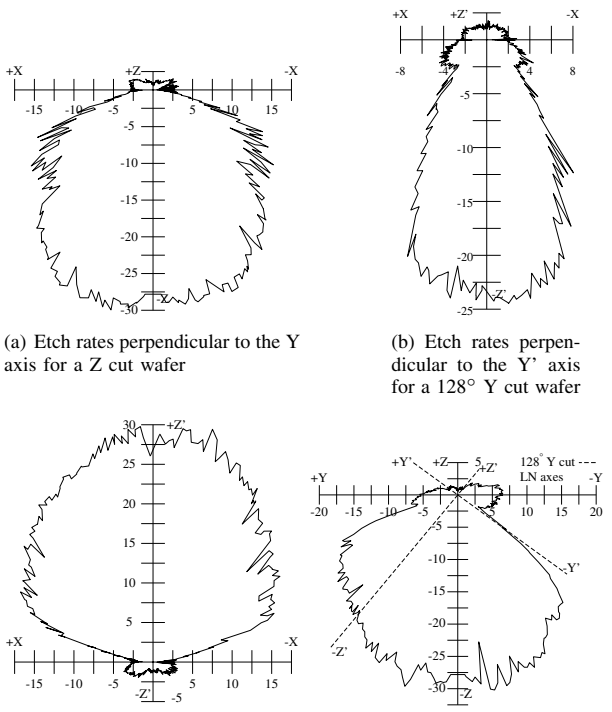

(a) Etch rates perpendicular to the Y axis for a Z cut wafer

(b) Etch rates perpendicular to the Y' axis for a 128° Y cut wafer

(c) Etch rates perpendicular to the Y' axis for a 163° Y cut wafer

(d) Etch rates perpendicular to the X axis for a Z cut wafer

Fig. 5. Various Wulff-Jaccodine plots for different crystal cuts. All of the graphs show the etch rate in μm/h.

circle represents the angle θ in Fig. 2(b). The data collected from the etched spheres will be made available at www.mems.mech.tohoku.ac.jp/esashilab/lnetchrate/etchrate.html.

From the etch diagrams, it can be seen that the etching exhibits a three-fold symmetry about the Z axis and the maximum etch rate is on –Z face, i.e. the $(000\bar{1})$ plane. Another detail to note between the two etch profiles is that the etch rate is more uniform for the HF etched sphere than for the HF:HNO_3 etched sphere.

To correct inaccuracies in determining the sphere center after etching, a Z cut wafer was etched and then compared to the results given by the spheres. The sphere data was then corrected to reflect the etch rates determined by the wafer. Without this correction, the etch rate on the +Z face was 25% that of the –Z face. It is generally accepted and has been confirmed by personal experiments that, the etch rate on the +Z face is less than 0.1% of the etch rate on the –Z face.

The crystal planes were calculated and then overlaid onto the etch data. It was found that crystal planes in the family of $(\bar{2}20\bar{3})$ planes showed the lowest etch rate in the –Z hemisphere. This crystal plane is close to the $(\bar{1}10\bar{2})$ plane, which is parallel to layers of Nb, Li and O atoms.

A. Etching Simulation

The data from the HF etched sphere is divided into three symmetry zones. Those zones are averaged into one symmetry zone, and then copied back to the other zones to form a full sphere of data. This helps to reduce the amount of noise in the data and remove the blank area where the orientation flat was located.

Next, the averaged data is rotated to the correct orientation needed for crystal cut being used. Then the etch rate data perpendicular to the X, Y or Y' axis is selected from the sphere and plotted. In Fig. 5 Y' and Z' refer to the rotated crystal axes and X, Y and Z refer to unrotated crystal axes. Examples of these plots for several different crystal cuts are shown in Fig. 5. In Fig. 5(d), only one plot along the Y axis is given because most crystal cuts for $LiNbO_3$ are rotated off the Y axis. In the figure, the crystal axes for a 128° Y cut wafer are shown, as an example. The etch rate for other crystal cuts can be obtained by rotating the crystal axes. In Figs. 5(a) through 5(c) a separate set of data is selected for each crystal cut.

Once etch distribution across a single crystal axis is plotted, the Wulff-Jaccodine method can be applied [11]. In Fig. 6 is an example of the Wulff-Jaccodine method used to predict the final shape of an etched 128° Y cut wafer.

The Wulff-Jaccodine method has two parts. The first part states that the final etched shape will minimize the free surface energy. The surface energy can be shown using the etch rate for the different crystal orientations. This first part will only predict the final planes revealed during the etching; however it does not predict the shape of more complex structures.

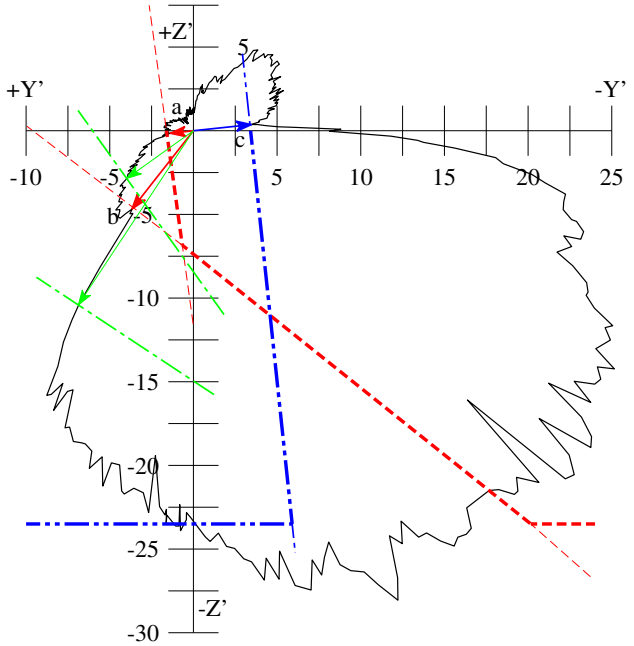

(a) Wulff-Jaccodine distribution rotated for a 128° Y cut wafer. The angles shown are a = 6.3°, b = 51.8°, and c = 6.0°.

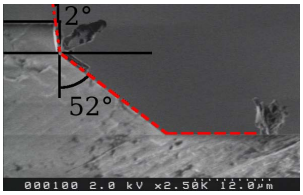

(b) Etched sample on the +Y side

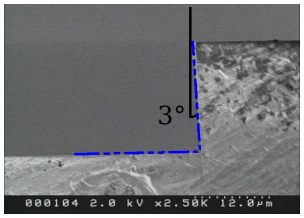

(c) Etched sample on the -Y side

Fig. 6. Etched shapes (a) predicted by the Wulff-Jaccodine method and (b, c) obtained by experiment

The second part of the Wulff-Jaccodine method is a geometric based rule. That rule states that when a line is drawn from the center of the surface energy diagram (etch rate diagram) to any point on the surface energy map, the line normal to that initial line cannot intersect any part of the final etched shape. An example of this is shown in Fig. 6(a). In Fig. 6(a), the thick dashed red lines and the thick dash-dot-dot blue lines are the final etched shape. The green dash-dot lines show examples of crystal planes that are not exposed because they do not meet the geometric rule. This geometric rule is what defines the shape of the final etched structure. The dashed red lines in Fig. 6(a) match with the exposed crystal planes shown in Fig. 6(b). The geometric rule makes it possible to model the complex structures made up of multiple crystal planes.

In Fig. 6, the etched shape is compared to the shape predicted by the Wulff-Jaccodine method. The etched shape predicted by the Wulff-Jaccodine model showed good agreement with the profile of the etched wafer. This shows that the etch rate data can be used with more advanced modeling programs.

The differences between the measured angle of the crystal planes and the those predicted using the Wulff-Jaccodine method arise from errors in the alignment of crystal axes and errors in measurement of the angles on the etched sample. The errors in the alignment of the crystal axes could be addressed by improving the center finding of the etched sphere, along with better alignment marks. The errors are less than 4.3° and can be accounted for by the previously discussed misalignments.

IV. Summary

Fundamental research into the etching characteristics of $LiNbO_3$ was carried out. The data was collected by etching 30 mm diameter spheres of $LiNbO_3$ with hydrofluoric and a mixture of hydrofluoric acid and nitric acid. The etch rate was plotted giving the etch rate over the entire sphere. The data can be downloaded at www.mems.mech.tohoku.ac.jp/esashilab/lnetchrate/etchrate.html. This data was used to predict the shape of etched wafers with the Wulff-Jaccodine method. The predicted shape agreed with those found from the etched wafers.

Acknowledgments

This work was supported in part by the Strategic Information and Communications R&D Promotion Programme (SCOPE) from the Ministry of General Affairs, Japan (No. 062302002). I would like to thank Jan Kuypers for his suggestions on this research.

References

[1] D. Cheng, K. Sato, M. Shikida, A. Ono, K. Sato, K. Asaumi, and Y. Iriye, "Characterization of Orientation-Dependent Etching Properties of Quartz: Application to 3-D Micormachining Simulation System," *Sensors and Materials*, vol. 17, no. 4, pp. 179–186, 2005.

[2] K. Sato, M. Shikida, Y. Matsushima, T. Yamashiro, K. Asaumi, Y. Iriye, and M. Yamamoto, "Characterization of orientation-dependent etching properties of single-crystal silicon: effects of KOH concentration," *Sensors and Actuators A*, vol. 64, pp. 87–93, 1998.

[3] K. Sato, M. Shikida, T. Yamashiro, K. Asaumi, Y. Iriye, and M. Yamamoto, "Anisotropic etching rates of single-crystal silicon for TMAH water solution as a function of crystallographic orientation," *Sensors and Actuators A*, vol. 73, pp. 131–127, 1999.

[4] J. Ray C. Ellis, "Etching of Single Crystal Germanium Spheres," *J. Appl. Phys.*, vol. 25, no. 12, pp. 1497–1499, 1954.

[5] P. Holmes, "The Orientation Dependence of Etching Effects on Germanium Crystals," *Acta Metallurgical*, vol. 7, pp. 283–289, 1959.

[6] F. Frank, "Orientation-Dependent Dissolution of Germanium," *J. Appl. Phys.*, vol. 31, no. 11, pp. 1996–1999, 1960.

[7] J. H. Kuypers, M. E. Schmidt, S. Tanaka, and M. Esashi, "Monolithic Phase Shifter Based on Mechanically Tunable SAW Based Delay Line," in *Transducers & Eurosensors*, vol. 1, Lyon, France, 2007, pp. 161–164.

[8] H. A. C. Tilmans, W. D. Raedt, and E. Beyne, "MEMS for wireless communications: 'from RF-MEMS components to RF-MEMS-SiP'," *Journal Of Micromechanics And Microengineering*, vol. 13, no. 4, pp. S139–S163, 2003.

[9] M. Fang, K. Vetelino, M. Rothery, J. Hines, and G. C. Frye, "Detection of organic chemicals by SAW sensor array," *Sensors And Actuators B-Chemical*, vol. 56, no. 1-2, pp. 155–157, 1999.

[10] H. Seidel, L. Csepregi, A. Heuberger, and H. Baumgärtel, "Anisotropic etching of crystalline silicon in alkaline solutions," *J. Electrochem. Soc.*, vol. 137, no. 11, pp. 3612–3626, 1990.

[11] R. Jaccodine, "Use of Modified Free Energy Theorems to Predict Equilibrium Growing and Etching Shapes," *J. Appl. Phys.*, vol. 33, no. 8, pp. 2643–2647, 1962.